

Article

Effect of Austenite-to-Ferrite Phase Transformation at Grain Boundaries on PWHT Cracking Susceptibility in CGHAZ of T23 Steel

Seong-Hyeong Lee ¹, Hye-Sung Na ², Kyong-Woon Lee ³, Jeong-yong Lee ² and Chung Yun Kang ^{2,*}

¹ Department of Hybrid Materials & Machining Technology, Graduate School of Convergence Science, Pusan National University, Busan 46241, Korea; reach486@naver.com

² Department of Material Science and Engineering, Pusan National University, Busan 46241, Korea; joyclubman@daum.net

³ Corporate R&D Institute, Doosan Heavy Industries, Changwon 642-792, Korea; kyongwoon.lee@doosan.com

* Correspondence: kangcy@pusan.ac.kr; Tel.: +82-10-8329-8429

Abstract: The post-weld heat treatment (PWHT) cracking susceptibility of a coarse grain heat-affected zone (CGHAZ) in SA213-T23 (2.25Cr-1.6W steel), used for boiler tubes employed in thermal power plants, was investigated using a Gleeble thermal cycle simulator. The PWHT cracking susceptibility test was performed at 650 °C, 700 °C and 750 °C, and it can be judged that the lower the reduce of area, the more susceptible it is to PWHT cracking. The results of the test also showed higher cracking susceptibility at 650 °C and 700 °C, mostly involving intergranular fracture, while at 750 °C, transgranular fracture was exhibited. Therefore, the PWHT cracking susceptibility is considered to be closely related to grain boundary. The microstructure of the simulated CGHAZ and PWHT at 650 °C, 700 °C and 750 °C was observed after etching with nital and alkaline sodium picrate etchants. Alkaline sodium picrate etched microstructures showed a white band at the grain boundary at 650 °C, 700 °C and 750, that did not appear in nital etching. Analysis of the white band using EPMA, TEM and nanoindentation revealed that it was intergranular ferrite depleted with C, W and Cr as compared to that in the matrix. Based on these results, we investigated the mechanism of intergranular ferrite formation during PWHT and its effect on PWHT cracking susceptibility at 650 °C, 700 °C and 750 °C.

Keywords: SA213-T23; cr-mo steel; CGHAZ; PWHT cracking; intergranular ferrite; Tint etching

1. Introduction

In order to achieve higher efficiency of thermal power plants, pipes and tubes used therein are increasingly required to sustain higher temperatures and pressures[1,2]. Therefore, SA213-T23 (2.25Cr-1.6W steel), which has better high-temperature creep strength than SA213-T22 (2.25Cr-1Mo steel), has been developed as a candidate material.

To develop SA213-T23 (2.25Cr-1.6W steel), the SA213-T22 (2.25Cr-1Mo steel) was modified by addition of tungsten (1.6%), reduction of molybdenum (0.2%) and carbon content (0.04-0.10%) and small additions of vanadium, nitrogen and boron[3-7].

However, in the case of T23 material, PWHT cracking (reheat cracking) has been reported in the process of post-weld heat treatment (PWHT) to mitigate the residual stress in the weld metal[8-16]. Therefore, much research has been conducted to analyze the cause of formation of reheat cracks in 2.25Cr-1.6W steel. JG Nawrocki et al explained that the cause of reheat cracking is due to weakening of the grain boundary by (1) the Cr- and W-depleted zones formed by the M3C and M23C6 carbides of Fe, Cr, and W in the grain boundaries[12,13], (2) the precipitation of an incoherent intergranular carbide M3C at the boundaries[4,5], (3) the grain boundary segregation of the Al and P elements[11,12]

and (4) transgranular strengthening by the homogeneous precipitation of a fine metal carbide containing the alloying elements V and Nb[11-13].

The previous studies had been carried out from the viewpoint that the alloy components of the matrix are homogeneous. However, research of M. Belde et al recently found that there is a microsegregation in the matrix where the alloying elements are not uniform, which can affect the mechanical properties and cause cracking in the course of the heat treatment[17,18]. According to Lee et al, the M23C6 precipitate of the base metal in 2.25Cr-1Mo-Ti steel partially dissolves in the thermal cycle of CGHAZ, and the microsegregation of C and Cr appears as a black stripe[19,20]. It is considered that such a microsegregation can affect the mechanical properties of PWHT due to phase transformation other than the matrix.

Many researchers have studied reheat cracking, but this study aims to investigate the effect of micro segregation on the reheat cracks in the matrix during PWHT, as there has been very little research on this aspect.

2. Materials and Methods

Table 1 presents the chemical composition of the SA213-T23 (2.25Cr-1.6W) material used in this study, which was analyzed using an optical emission spectrometer (LAB LAVM 10, SPECTRO Analytical Instruments GmbH, Kleve, Germany).

Table 1. Chemical composition of the T23 steel.

Material	Chemical Composition (at. %)														
	C	Si	Mn	Ni	Cr	Mo	V	Nb	Al	Ti	B	W	N	Fe	
SA213-T23	0.07	0.24	0.50	0.11	2.09	0.15	0.22	0.028	0.018	0.042	0.0017	1.66	0.0095	Bal	

In actual welding, it is impossible to carry out the evaluation of the mechanical properties because the HAZ is a narrow region owing to various thermal cycles. Therefore, the PWHT cracking test was performed by using the Gleeble 3500 (Dynamic Systems Inc., New York, NY, USA) thermal cycle simulator to reproduce the thermal cycle curve (1350°C peak) of CGHAZ which was calculated by using the Sysweld software 9.5 (ESI, Paris, France) for simulation of the welding analysis. The welding conditions used in the Sysweld calculations are as follows: weld method: Gas tungsten arc welding (GTAW), heat input: 16 kJ / cm, thickness: 6 mm

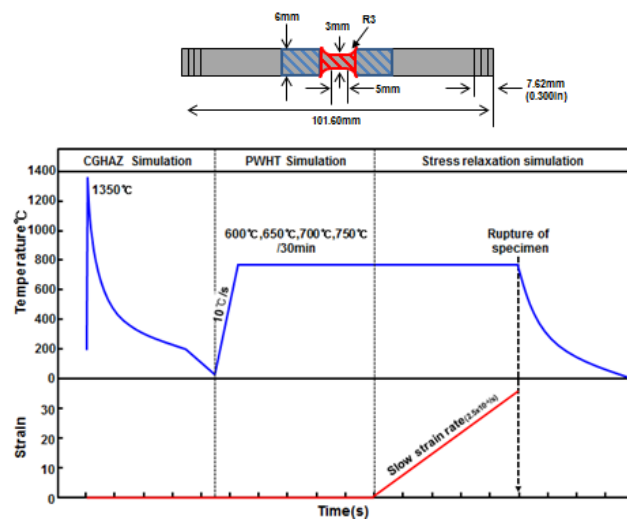


Figure 1. Schematic illustration of PWHT cracking susceptibility test at various PWHT temperatures and geometry of the sample.

Figure 1 shows the schematic diagram and specimen geometry of the PWHT cracking test. After 30 min at PWHT temperatures (600°C, 650°C, 700°C, 750°C), the tensile test was performed at a very

low strain rate (2.5×10^{-4}). As a result of the PWHT test, if the reduction in area is low, it is concluded that cracking is likely to occur because of low grain boundary ductility, and sensitivity to reheat cracking is higher. The reason for the tensile test at a very low strain rate (2.5×10^{-4}) is to prevent plastic deformation before the brittle fracture mode due to PWHT cracking.

The microstructure of the simulated CGHAZ and PWHT was observed by etching it with nital etchant (2 mL HNO₃, 50 mL methanol) and alkaline sodium picrate etchant (2 g picric acid, 25 g NaOH, 100 mL boiled water). The fracture surface was observed by using a scanning electron microscope (SEM) (SUPRA40VP, Carl Zeiss, Oberkochen, Germany). The phase analysis of the simulated CGHAZ and PWHT was performed using an electron probe micro-analyzer (EPMA) (JXA-8530F, JEOL, Tokyo, Japan) and field-emission transmission electron microscope (FE-TEM) (TALOS F200X, FEI, Hillsboro, OR, USA), and the time-temperature-transformation diagram (TTT diagram) was obtained by using JMatPro 5.1 software (Sente Software, Surrey Research Park, United Kingdom) to analyze the experimental results.

Thin-film specimen of CGHAZ for TEM analysis was prepared by mechanical polishing, followed by jet electro polishing using an electrolyte consisting of a mixture of 95% methanol and 5% perchloric acid, maintained at a temperature of 20°C. Thin-film of 700°C specimen was prepared using the focused ion beam (FIB) (FEI Scios, Thermo Fisher Scientific, Hillsboro, OR, USA).

The transgranular hardness was measured using a Vickers hardness tester (HM-200, Mitutoyo Corporation, Kanagawa, Japan), and the hardness near the grain boundaries by using a nanoindenter (TI-950, HYSITON, Minneapolis, United States).

3. Results and Discussion

3.1. PWHT Cracking Susceptibility Test

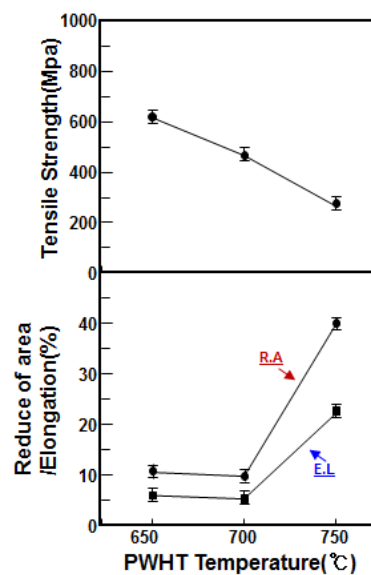


Figure 2. Results of PWHT cracking test at various temperatures.

Figure 2 shows the results of the PWHT cracking susceptibility test of CGHAZ at various temperatures. The test was performed by holding the simulated CGHAZ at PWHT temperatures (650°C, 700°C, 750°C) for 30 min and then the tensile test was performed under the strain rate condition of 2.5×10^{-4} .

As the PWHT temperature increases, the tensile strength tends to decrease almost linearly to 619 MPa, 466 MPa and 278 MPa at 650°C, 700°C and 750°C, respectively. On the other hand, the reduction in area and elongation are low at 10.4% and 5.9% at 650°C and 9.7% and 5.2% at 700°C, respectively.

However, the reduction in area and elongation at 750°C increased to 40.0% and 22.5%, respectively. It is found that the lower the reduction in area, the more the susceptibility to PWHT cracking[21-23]; in other words, CGHAZ is susceptible to PWHT cracking at 650°C and 700°C, but not at 750°C.

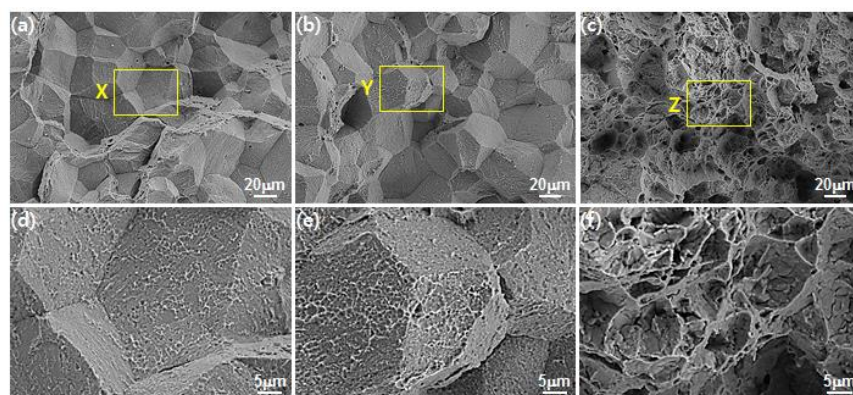


Figure 3. Representative SEM photomicrographs of the fracture surfaces of specimens that failed during testing at (a) 650°C (b) 700°C and (c) 750°C. Enlarged SEM photomicrographs (d), (e), (f) at regions denoted by X, Y, Z.

In order to analyze the correlation between PWHT cracking susceptibility and fracture surface, the fracture surfaces of specimens that failed during the testing at 650°C, 700°C and 750°C were observed by SEM as shown in Figure 3. The surfaces at 650°C and 700°C shown in Figures 3 (a) and (b) largely appear as intergranular fractures which are generally sensitive to PWHT and considered to have lower intergranular strength than transgranular strength. Figures 3 (d) and (e) are the enlargements of the X and Y regions in Figures 3 (a) and (b), respectively, and show that the grain boundaries are covered by fine dimples. The surface at 750°C shown in Figure 3 (c), which is not sensitive to PWHT cracking, mostly appears as transgranular fracture. Therefore, it is considered that the intergranular strength is not lower than transgranular strength at 750 ° C. As a result of the fracture surface analysis, the reheat cracking sensitivity is considered to be correlated with intergranular and transgranular strengths.

3.2 Correlation between Microstructure and PWHT Cracking Susceptibility

Figure 4 shows the optical microscopic structure of CGHAZ at PWHT temperatures (650°C, 700°C, 750°C) using nital and alkaline sodium picrate etching. In order to compare the differences between nital and alkaline sodium picrate etching, the microstructure was observed after nital etching, and it was subsequently finely polished. Afterward, alkaline sodium picrate etching was performed to observe the same position as that observed in nital etching, and the differences in the microstructures owing to etching.

The nital-etched microstructure of CGHAZ reveals the prior austenite grain boundary and lath in the matrix. The PWHT conditions at 650°C, 700°C and 750°C also showed the prior austenite grain boundary and lath in the matrix, but the lath of the PWHT condition was thicker than that of CGHAZ due to the tempering effect.

The alkaline-sodium-picrate-etched microstructure of the CGHAZ also shows the prior austenite grain boundary and lath in the matrix, as in the case of nital etching, but with a black band that was not observed in nital-etched microstructure. According to Lee's study, the M23C6 precipitates of the base metal are due to partial dissolution in the CGHAZ thermal cycle and are not completely diffused, and the fine segregation of the remaining C, W, and Cr appears as a black band in the CGHAZ[19]. The grain boundaries of CGHAZ are observed as black lines. However, when PWHT is performed at 650°C, 700°C and 750°C, white bands appeared at the grain boundaries, which

was different from the observation in CGHAZ. There is also a black band at 650°C, 700°C and 750°C, which suggests that C, W, and Cr segregations of CGHAZ are not diffused even under PWHT. The presence of C, W, and Cr segregation in the PWHT was also examined in the EPMA analysis.

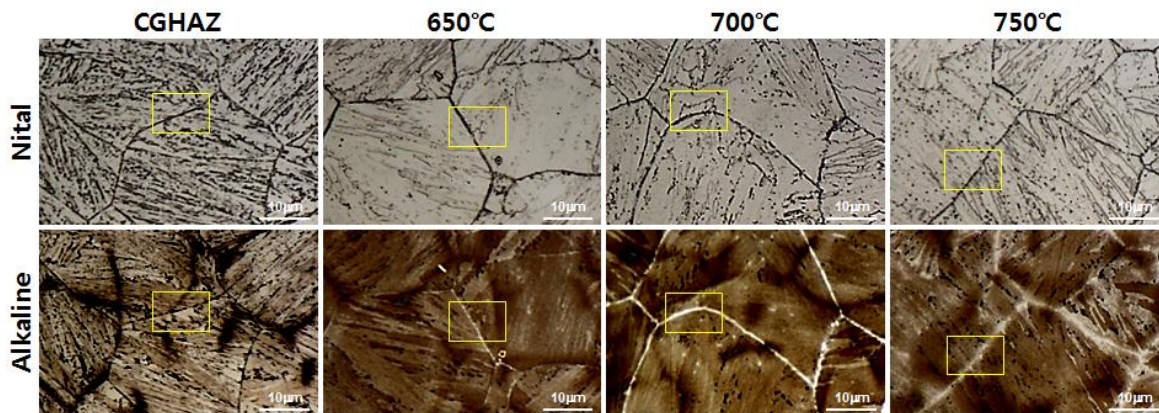


Figure 4. Optical microstructure with etchants (nital, alkaline sodium picrate) at various PWHT temperatures.

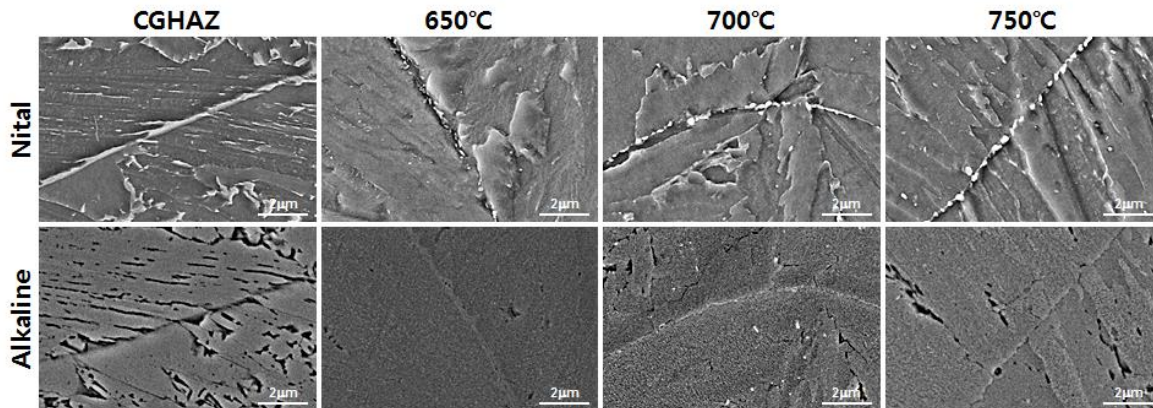


Figure 5. SEM microstructure with etchants (nital, alkaline sodium picrate) at various PWHT temperatures.

Figure 5 shows the SEM structure of the CGHAZ at PWHT temperatures (650°C, 700°C, 750°C) using nital and alkaline sodium picrate etching. The observed part is shown in Figure. 4 as the □ area. nital etched SEM microstructures show a line at the grain boundaries of the CGHAZ. However, in PWHT at 650°C, 700°C and 750 °C, precipitates were observed instead of lines at the grain boundaries. Therefore, it is considered that the line of CGHAZ is transformed into precipitate during PWHT.

On the other hand, in the alkaline sodium picrate etched microstructure, neither lines nor precipitates at grain boundaries in either CGHAZ or PWHT were observed clearly. In nital etching, the grain boundaries and precipitates are clearly visible because the matrix is reduced. However, they are not seen clearly in alkaline sodium picrate etching because the matrix is not reduced.

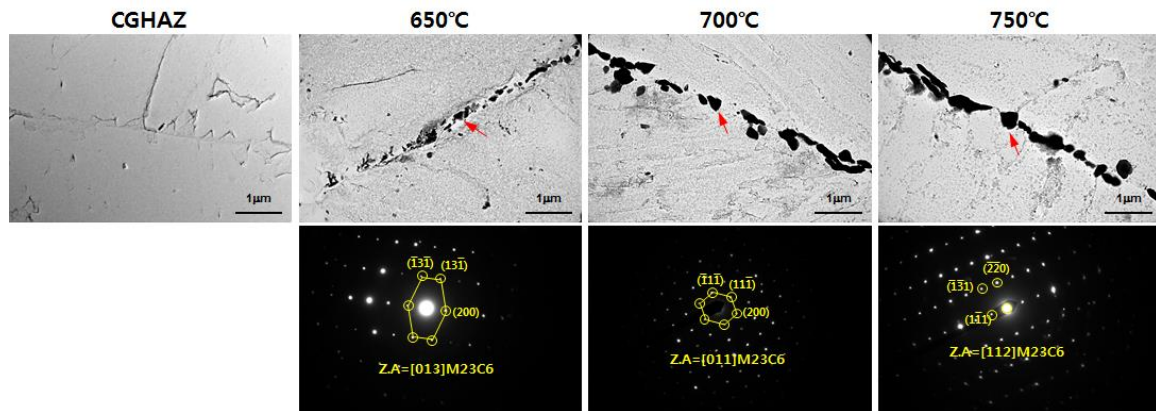


Figure 6. TEM microstructure and diffraction pattern at the regions denoted by arrows at various PWHT temperatures

Figure 6 shows the results of the TEM analysis of the precipitates using the carbon replica method in order to identify the phases of the precipitates at the grain boundaries at PWHT temperatures. The diffraction pattern of the line at the grain boundaries in CGHAZ could not be obtained, and it was considered that it was not extracted from the carbon replica. The PWHT conditions at 650°C, 700°C and 750°C showed precipitates at the grain boundaries, and the diffraction pattern analysis of these revealed that it was M23C6 carbide. Observation of the microstructure shows that a line exists at the grain boundaries of CGHAZ, and white bands and M23C6 appear at 650°C, 700°C and 750°C when PWHT is performed.

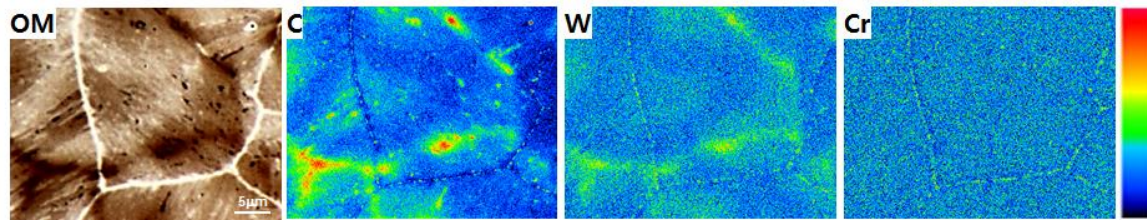


Figure 7. EPMA mapping results showing the distribution of elements at 700°C

Figure 7 shows the results of EPMA mapping for analyzing the alloy compositions of the white bands and M23C6 carbide at the grain boundaries and the black band, at 700°C. The white band at the grain boundary at 700°C can be observed to be depleted of C; W and Cr are not clearly visible but appear to be depleted. The M23C6 intergranular precipitates inside the white band are concentrated in C, W and Cr. It is considered that the depleted zone is formed around the M23C6 precipitate because the M23C6 carbide with high C, W and Cr components precipitates at the grain boundary[24-27] when PWHT is carried out at 700°C. According to a study by Lee et al, the black band in alkaline sodium picrate etched CGHAZ is the segregated region of C, W, and Cr[19,20]. The black band at 700°C is also a region where C, W, and Cr components are concentrated. It can be seen that even if PWHT is performed, C, W and Cr are not diffused but remain as segregation regions. To summarize, at 700°C, the white band of the grain boundaries is a C, W, and Cr depleted zone, and M23C6 precipitates in which C, W, and Cr components are concentrated, are present in the white band and the black band is an area concentrated in C, W, and Cr. At 650°C and 750°C, it can be considered that the white band is the region where C, W, and Cr are depleted, and the black band is a region where C, W and Cr are concentrated.

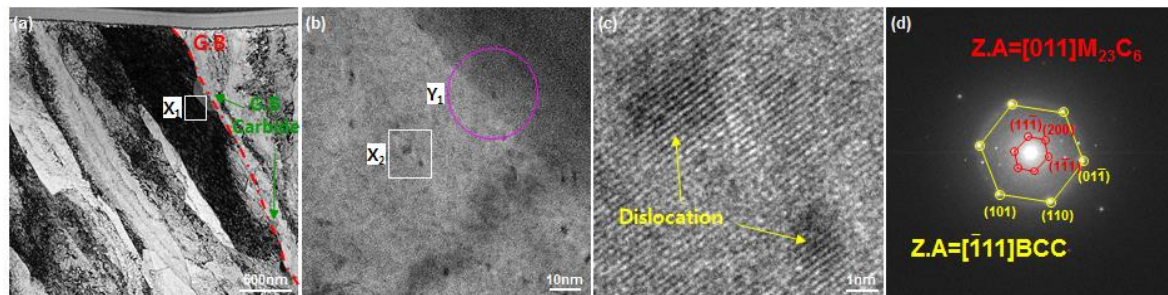


Figure 8. (a) TEM micrograph at 700°C (b) Enlarged micrograph of the region denoted by X¹, (c) HR-TEM micrograph of the region denoted by X² (d) Diffraction pattern of the region denoted by Y¹

In order to identify the phase of the white band at the grain boundary, the specimen was prepared using FIB of grain boundaries at 700°C and observed using TEM. In the low-magnification TEM photograph of Figure 8, bands and precipitates are observed at the grain boundary. In Figure 8 (b), which is an enlarged view of the region X¹ of the grain boundary, a black dot is observed inside the band which looks like a precipitate or dislocation. However, in the HR image of Fig. 8 (c), which enlarges the X² region of Fig. 8 (b), the band and black dot have the same atomic arrangement. Therefore, the black spot inside the band is judged to be a dislocation, and not a precipitate. A diffraction pattern analysis of the Y¹ region was performed to identify the phase of the bands and precipitates. As a result of the analysis, the band of the grain boundary which was a BCC structure, was judged to be intergranular ferrite because there was no transgranular precipitation, although there was dislocation, and the precipitate of the grain boundary was M₂₃C₆.

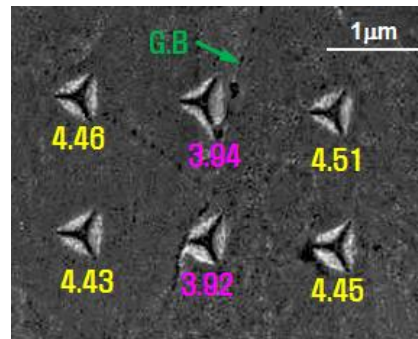


Figure 9. Nanoindentation results showing hardness at 700°C

Figure 9 is the result of the analysis with a nanoindenter to compare the hardness of the intergranular ferrite with the matrix at 700°C. In order to measure the hardness of intergranular ferrite with thickness of 1.0 ~ 1.2 μm, the indenter size was tested to be 0.5 μm or less. As a result of the nanoindentation analysis, it can be seen that the hardness of intergranular ferrite is 3.92~3.94 Gpa, which is lower than that of the matrix, which is 4.43 ~ 4.51 Gpa. As a result of EPMA, nanoindentation and TEM analysis, the white band at the grain boundary in alkaline sodium picrate etching at 650°C, 700°C and 750°C is identified to be intergranular ferrite where C, W, and Cr are depleted more than in the matrix, and intergranular ferrite has lower hardness than the matrix at 700°C.

Therefore, it is considered that ductile intergranular ferrite is generated in the grain boundary when PWHT is carried out at 700°C, thereby lowering the intergranular strength. This is the reason why intergranular fracture appears largely at 700°C and is sensitive to PWHT. The fracture surfaces at 650°C and 700°C in Figure 3 appear as intergranular fractures mostly covered with fine dimples at the grain boundaries, attributed to ductile intergranular ferrite, and sensitive to reheat cracks. However, the fracture surface at 750°C was mostly transgranular and not sensitive to reheat cracking.

It is considered that the intergranular strength is lower than transgranular strength at 650°C and 700°C. However, this is not the case at 750°C.

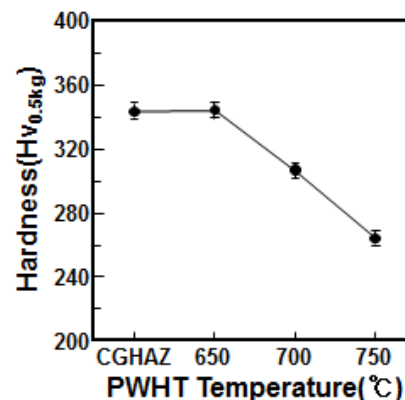


Figure 10. Comparison of matrix hardness at various PWHT temperatures

Figure 10 shows the Micro-Vickers hardness of the matrix for various PWHT temperatures. The matrix hardness at 650°C was similar to that of the CGHAZ despite PWHT, and decreased at 700°C and 750°C as the temperature increased. Generally, the greater the hardness, the greater the strength[28-30]. Therefore, it is expected that as the PWHT temperature increases, the transgranular strength decreases due to the tempering effect. Therefore, the transgranular strength at 700 °C is greater than the intergranular strength which is weakened by intergranular ferrite, but at 750 °C it is expected to be similar to or lower than the intergranular strength.

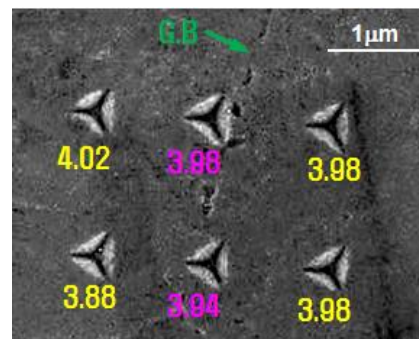


Figure 11. Nanoindentation results showing hardness at 750°C.

Figure 11 shows the results of nanoindentation analysis to compare the hardness of intergranular ferrite and the matrix at 750°C. The analysis shows that the hardness of the matrix at 700°C is 3.88~4.02 Gpa, which is similar to that of intergranular ferrite, which is 3.94~3.98 Gpa. It is considered that the transgranular strength at 750 °C is similar to the intergranular strength. Therefore, at 750 °C, the grain boundary is softened by intergranular ferrite, but the matrix is softened similarly at the grain boundary, so that intergranular fracture did not occur and CGHAZ was not sensitive to PWHT cracking.

3.3 Formation Mechanism of Ferrite at Prior Austenite Grain Boundary

Figure 12 shows the results of the EPMA surface analysis for analyzing the alloy composition of the grain boundary and black band of CGHAZ. The black band of CGHAZ is a region where C, W, and Cr components are concentrated. Lee's study showed that the M23C6 of the matrix in the CGHAZ

thermal cycle dissolves but is not fully diffused, revealing C, W, and Cr segregations. The line at the grain boundaries of the CGHAZ observed in the SEM microstructure of Fig. 5 is the region where C is concentrated.

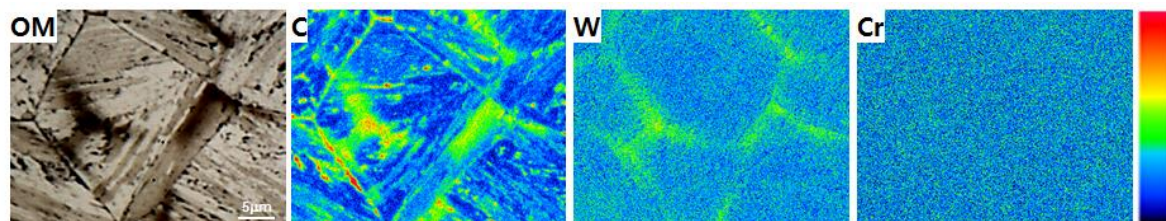


Figure 12. EPMA mapping results showing the distribution of elements in CGHAZ.

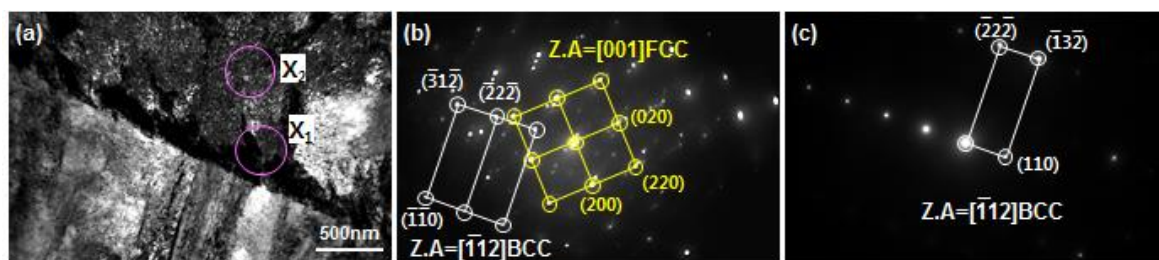


Figure 13. (a) TEM micrograph of CGHAZ; (b) and (c) Diffraction patterns at the regions denoted by X^1 and X^2

In order to identify the phase of the line at the grain boundary of CGHAZ, a thin film was prepared and observed using TEM. In the BF image of Fig. 13 (a), the line at the grain boundary is seen. A diffraction pattern analysis of the X^1 and X^2 regions was performed to identify the phases of the line at the grain boundary and the matrix. As a result of the analysis, the line at the grain boundary was found to be austenite of FCC structure and the matrix was of BCC structure, which was determined to be martensite considering the rapid cooling rate and hardness (340 Hv) of CGHAZ. To conclude, the result of the EPMA and TEM analysis indicated that the line at the grain boundary of CGHAZ was austenite with carbon concentration.

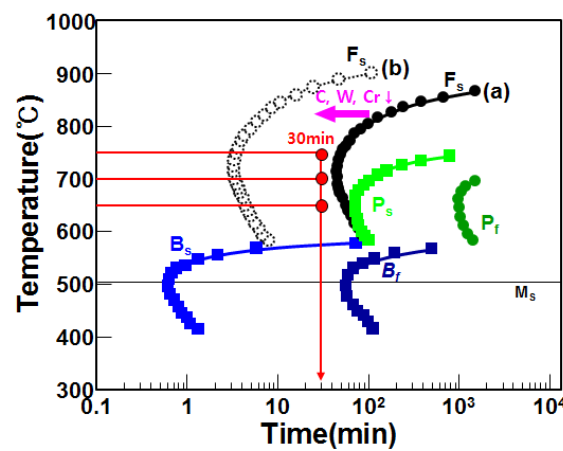


Figure 14. Time-temperature transformation (TTT) diagrams for alloy composition of matrix (Fe-0.07%C-2.09Cr-1.66W) calculated with JMatPro software. (a) Ferrite nose time of matrix alloy composition (b) Predicted ferrite nose time when C, W, Cr is depleted

In order to investigate the reason for generation of intergranular ferrite during PWHT, the TTT-curve, according to the alloy composition of the matrix, was obtained, as shown in Figure 14, by using

JmatPro simulation. In the case of PWHT of the alloy composition of the matrix for 30 min at 650°C, 700°C and 750°C, the austenite at the grain boundary of CGHAZ does not transform into ferrite because the ferrite nose time is longer than 30 min. However, the grain boundaries are regions where the C, W, and Cr components are depleted by the M23C6 precipitation, due to which the ferrite nose time decreases[31]. In such a situation, austenite at the grain boundary of CGHAZ transforms into intergranular ferrite.

4. Conclusions

PWHT cracking susceptibility and microstructural characteristics of CGHAZ in SA213-T23 were investigated at various PWHT temperatures. The findings are summarized as follows:

(1) As a result of the PWHT cracking susceptibility test of CGHAZ at 650°C, 700°C and 750°C, it was found that CGHAZ was sensitive to PWHT at 650°C and 700°C but not at 750°C. The surfaces at 650°C and 700°C contain intergranular fractures, but at 750°C they contain transgranular fractures.

(2) In order to investigate the microstructural characteristics of CGHAZ at PWHT temperatures, microstructures were observed by etching with nital and alkaline sodium picrate etchants. Alkaline-sodium-picrate-etched microstructures at 650°C, 700°C and 750°C showed white bands at grain boundaries that did not appear in nital etching. In the EPMA and TEM analyses, the white band at the grain boundaries of 650°C, 700°C and 750°C was intergranular ferrite depleted in C, W and Cr.

(3) The reason why intergranular fracture appears largely at 650°C and 700°C and is sensitive to PWHT cracking is that the intergranular strength is lower than the transgranular strength due to ductile intergranular ferrite. At 750°C, surface fracture is mostly transgranular fracture and is not susceptible to PWHT cracking. The reason is that the intergranular ferrite lowers the intergranular strength, but the transgranular strength is also lowered by the high tempering effect, so that the intergranular strength and the transgranular strength are similar to each other.

(4) A line observed at the grain boundary of CGHAZ was found to be austenite with carbon concentration, on the basis of EPMA and TEM analysis.

(5) In the case of PWHT of the alloy composition of the matrix for 30 min at 650°C, 700°C and 750°C, the austenite at the grain boundary of CGHAZ does not transform into ferrite because the ferrite nose time in TTT-curve is longer than 30 min. However, the grain boundary is a region where C, W, and Cr are depleted by M23C6 precipitation with high C, W, and Cr components. When C, W, and Cr are depleted, the ferrite nose time becomes shorter than 30 min, so that austenite at the grain boundary of CGHAZ is then transformed into ferrite.

Acknowledgments: This work was supported by a National Research Foundation of Korea (NRF) grant funded by the Korea government (MSIP) (No. 2012R1A5A1048294).

Author Contributions: Seong-Hyeong Lee, Hye-Sung Na, Kyong-Woon Lee and Chung-Yun Kang conceived and designed the experiments; Seong-Hyeong Lee and Jeong-yong Lee performed the experiments; Seong-Hyeong Lee, Hye-Sung Na and Chung-Yun Kang analyzed the data; Seong-Hyeong Lee wrote this paper.

Conflicts of Interest: The authors declare no conflict of interest. The funding sponsors had no role in the design of the study; in the collection, analyses, or interpretation of data; in the writing of the manuscript, and in the decision to publish the results.

References

1. Klueh, R.; Nelson, A. Ferritic/martensitic steels for next-generation reactors. *Journal of Nuclear Materials* **2007**, *371*, 37-52.
2. Bendick, W.; Gabrel, J.; Hahn, B.; Vandenberghe, B. New low alloy heat resistant ferritic steels t/p23 and t/p24 for power plant application. *International Journal of Pressure Vessels and Piping* **2007**, *84*, 13-20.
3. Haarmann, K.; Kottmann, G.; Vaillant, J. The t23/24 book. **2000**.
4. Nawrocki, J.; Dupont, J.; ROBINO, C.V.; Marder, A. *The stress-relief cracking susceptibility of a new ferritic steel-part i: Single-pass heat-affected zone simulations*; Sandia National Labs., Albuquerque, NM (US); Sandia National Labs., Livermore, CA (US): 1999.
5. Nawrocki, J.; Dupont, J.; Robino, C.; Puskar, J.; Marder, A. The mechanism of stress-relief cracking in a ferritic alloy steel. *WELDING JOURNAL-NEW YORK-* **2003**, *82*, 25-S.
6. Masuyama, F.; Yokoyama, T.; Sawaragi, Y.; Iseda, A. Service exposure and reliability improvement: Nuclear, fossil, and petrochemical plants. PVP: 1994.
7. Jiménez, J.A.; Carsí, M.; Ruano, O.A. Effect of rhenium on the microstructure and mechanical behavior of fe-2.25 cr-1.6 w-0.25 v-0.1 c bainitic steels. *Journal of Materials Science & Technology* **2017**, *33*, 1487-1493.
8. Di Gianfrancesco, A. *Materials for ultra-supercritical and advanced ultra-supercritical power plants*. Woodhead Publishing: 2016.
9. Wang, B.; Xueyuan, X.; Feng, Z.; Anfang, Q.; Zhengran, L.; Bo, Z.; Yongqiang, J.; Xiaoli, L. In *Research on water wall tubes and welded joints of 1000 mw usc tower boiler*, 7th International Conference on Advances in Materials Technology for Fossil Power Plants, 2013.
10. Viswanathan, R. *Advances in materials technology for fossil power plants: Proceedings from the fifth international conference, october 3-5, 2007, marco island, florida, USA*. ASM International: 2008.
11. Heo, N.; Chang, J.; Kim, S.-J. Elevated temperature intergranular cracking in heat-resistant steels. *Materials Science and Engineering: A* **2013**, *559*, 665-677.
12. Park, K.; Kim, S.; Chang, J.; Lee, C. Post-weld heat treatment cracking susceptibility of t23 weld metals for fossil fuel applications. *Materials & Design* **2012**, *34*, 699-706.
13. Chang, J.; Kim, B.; Heo, N. Stress relief cracking on the weld of t/p 23 steel. *Procedia Engineering* **2011**, *10*, 734-739.
14. Heo, N.; Chang, J.; Yoo, K.; Lee, J.; Kim, J. The mechanism of elevated temperature intergranular cracking in heat-resistant alloys. *Materials Science and Engineering: A* **2011**, *528*, 2678-2685.
15. Chang, J.; Heo, N.; Lee, C. Intergranular cracking susceptibility of 2.25 cr1. 3w and 9cr1movnb weld metals at elevated temperatures. *Metals and Materials International* **2010**, *16*, 981-985.
16. Chang, J.; Heo, N.; Lee, C. Effects of mo addition on intergranular cracking behavior of 2.25 crw (p23) weld metal at elevated temperatures. *Metals and Materials International* **2011**, *17*, 131-135.
17. Bilde, M.; Springer, H.; Inden, G.; Raabe, D. Multiphase microstructures via confined precipitation and dissolution of vessel phases: Example of austenite in martensitic steel. *Acta Materialia* **2015**, *86*, 1-14.
18. Raabe, D.; Sandlöbes, S.; Millán, J.; Ponge, D.; Assadi, H.; Herbig, M.; Choi, P.-P. Segregation engineering enables nanoscale martensite to austenite phase transformation at grain boundaries: A pathway to ductile martensite. *Acta Materialia* **2013**, *61*, 6132-6152.
19. Lee, K.; Lee, S.; Na, H.; Kang, C. Ghost microstructure evolution and identification in the coarse grain

heat affected zone of 2.25 cr-1mo-v-ti steel using tint etching. *Materials Characterization* **2016**, *121*, 31-39.

20. Lee, S.-H.; Na, H.-S.; Lee, K.-W.; Choe, Y.; Kang, C.Y. Microstructural characteristics and m23c6 precipitate behavior of the course-grained heat-affected zone of t23 steel without post-weld heat treatment. *Metals* **2018**, *8*, 170.

21. Dhooge, A.; Vekeman, J. New generation 2 1/4 cr steels t/p 23 and t/p 24 weldability and high temperature properties. *Welding in the World* **2005**, *49*, 75-93.

22. Shinya, T.; Tomita, Y. Effect of calcium treatments and strain rate on reheat cracking of vanadium-modified 2.25 cr-1mo steel. *Materials characterization* **1998**, *40*, 221-225.

23. Nevasmaa, P.; Salonen, J. Reheat cracking susceptibility and toughness of 2% crmowvn p23 steel welds. *Welding in the World* **2008**, *52*, 68-78.

24. Kaneko, K.; Fukunaga, T.; Yamada, K.; Nakada, N.; Kikuchi, M.; Saghi, Z.; Barnard, J.S.; Midgley, P.A. Formation of m23c6-type precipitates and chromium-depleted zones in austenite stainless steel. *Scripta Materialia* **2011**, *65*, 509-512.

25. Thorvaldsson, T.; Dunlop, G. Grain boundary cr-depleted zones in ti and nb stabilized austenitic stainless steels. *Journal of materials science* **1983**, *18*, 793-803.

26. Almubarak, A.; Abuhaimeed, W.; Almazrouee, A. Corrosion behavior of the stressed sensitized austenitic stainless steels of high nitrogen content in seawater. *International Journal of Electrochemistry* **2013**, *2013*.

27. Nakamichi, H.; Sato, K.; Miyata, Y.; Kimura, M.; Masamura, K. Quantitative analysis of cr-depleted zone morphology in low carbon martensitic stainless steel using fe-(s) tem. *Corrosion Science* **2008**, *50*, 309-315.

28. Gaško, M.; Rosenberg, G. Correlation between hardness and tensile properties in ultra-high strength dual phase steels—short communication. *Mater. Eng* **2011**, *18*, 155-159.

29. Shen, Y.-L.; Chawla, N. On the correlation between hardness and tensile strength in particle reinforced metal matrix composites. *Materials Science and Engineering: A* **2001**, *297*, 44-47.

30. Chenna, K.S.; Kumar, G.N.; Jha Abhay, K.; Bhanu, P. On the prediction of strength from hardness for copper alloys. *Journal of Materials* **2013**, *2013*.

31. Na, H.-s.; Kim, B.-h.; Lee, S.-h.; Kang, C.-y. Thermodynamic alloy design of high strength and toughness in 300 mm thick pressure vessel wall of 1.25 cr-0.5 mo steel. *Metals* **2018**, *8*, 70.